arXiv:0807.0581v2 [cond-mat.mes-hall] 20 Oct 2008

Transport properties and Kondo correlations in nanostructures: the time-dependent DMRG method applied to quantum dots coupled to Wilson chains

Luis G. G. V. Dias da Silva,[1] F. Heidrich-Meisner,[2] A. E. Feiguin,[3,4]
C. A. Büsser,[5] G. B. Martins,[5] E. V. Anda,[6] and E. Dagotto[1]

[1]*Materials Science and Technology Division, Oak Ridge National Laboratory, Oak Ridge, Tennessee 37831, USA and Department of Physics and Astronomy, University of Tennessee, Knoxville, Tennessee 37996, USA*
[2]*Institut für Theoretische Physik C, RWTH Aachen University, 52056 Aachen, and JARA – Fundamentals of Future Information Technology, Germany*
[3]*Microsoft Project Q, University of California, Santa Barbara, CA 93106, USA*
[4]*Condensed Matter Theory Center, Department of Physics, University of Maryland, College Park, Maryland 20742, USA*
[5]*Department of Physics, Oakland University, Rochester, Michigan 48309, USA*
[6]*Departamento de Física, Pontificia Universidade Católica do Rio de Janeiro (PUC-Rio), 22452-970, Caixa Postal: 38071 Rio de Janeiro, Brazil.*

(Dated: February 2, 2022)

We apply the adaptive time-dependent Density Matrix Renormalization Group method (tDMRG) to the study of transport properties of quantum-dot systems connected to metallic leads. Finite-size effects make the usual tDMRG description of the Kondo regime a numerically demanding task. We show that such effects can be attenuated by describing the leads by "Wilson chains", in which the hopping matrix elements decay exponentially away from the impurity ($t_n \propto \Lambda^{-n/2}$). For a given system size and in the linear response regime, results for $\Lambda > 1$ show several improvements over the undamped, $\Lambda = 1$ case: perfect conductance is obtained deeper in the strongly interacting regime and current plateaus remain well defined for longer time scales. Similar improvements were obtained in the finite-bias regime up to bias voltages of the order of the Kondo temperature. These results show that, with the proposed modification, the tDMRG characterization of Kondo correlations in the transport properties can be substantially improved, while it turns out to be sufficient to work with much smaller system sizes. We discuss the numerical cost of this approach with respect to the necessary system sizes and the entanglement growth during the time-evolution.

PACS numbers: 73.63.Kv,73.23.-b, 72.10.Fk, 72.15.Qm

I. INTRODUCTION

The current excitement in the condensed matter and materials science community surrounding the study of nanoscale transport stems from both the potential applicability in molecular electronic devices[1] and the possibility of designing nanostructures to realize quantum impurity Hamiltonians. Hallmark experimental achievements include the observation of the Kondo effect in quantum dots,[2,3] molecules,[4] nanotubes,[5,6] and non-Fermi liquid behavior in quantum dot structures.[7]

While transport is an intrinsic non-equilibrium situation, in the linear response regime transport coefficients are commonly derived from equilibrium correlation functions.[8,9] A prominent numerical tool for describing the equilibrium Kondo regime is Wilson's numerical renormalization-group method (NRG). In the original NRG formulation for the Kondo model,[10,11] Wilson showed that the contribution from band states exponentially close to the Fermi energy needs to be taken into account in order to capture the correct properties of the ground state. For this reason, standard tight-binding numerical approaches face a formidable challenge in addressing this problem: finite-size effects set a minimum energy scale, the level spacing, below which the calculation cannot capture the crossover to the Kondo state.[12,13,14]

Wilson proposed a combination of two elements to handle this problem: (i) A discretization procedure of the metallic band, leading to a mapping into a impurity connected to a one-dimensional tight-binding chain with exponentially decaying hoppings. We will refer to such leads as *Wilson chains* in this work. (ii) A non-perturbative renormalization procedure that probes successive energy scales by recursively diagonalizing the Hamiltonian and keeping the relevant states at each scale.

Recent theoretical[15,16,17,18,19,20,21,22,23,24,25,26,27,28,29,30,31] and experimental efforts[32] aim at observing and modeling genuine non-equilibrium physics. A particularly important question is under what conditions steady-state situations can be reached in numerical simulations, and promising results have been obtained using time-dependent approaches.[20,21,22,23,24,25] Such ideas have been pursued using both the density matrix renormalization group (DMRG) technique[33,34,35,36] and the NRG,[11,22,23,24] in the former case utilizing the adaptive time-dependent DMRG.[37,38]

Moreover, the incorporation of ingredients of DMRG into NRG and vice versa has led to a significant extension of both methods.[22,39,40,41,42,43] As a prominent example, this includes the use of Wilson chains in DMRG for the description of the Kondo regime of the Anderson impurity model in Refs. 40,41, where in Ref. 41 the common

mathematical structure of NRG and (single-site) DMRG in terms of matrix-product states has been exploited. Recently, a similar idea has been successfully explored within a cluster-embedding approach, resulting in the development of the so-called logarithmic discretization embedded cluster approximation (LDECA).[44]

The advantage of DMRG is its flexibility: it is in principle possible to model complex interacting regions[35] or to incorporate interactions into the leads (see, *e.g.*, Ref. 45). Moreover, it is the numerical method of choice for one-dimensional bulk systems, and it allows for the calculation of extended correlation functions in a straightforward way. For the description of transport phenomena, there is no restriction to work in the small bias regime, as finite biases can be incorporated into time-dependent simulations.[20,21,25]

In transport investigations based on DMRG, several groups have introduced modifications in the contact leads, such as the logarithmic discretization, to improve the results of either the ground state[40,41] or tDMRG calculations. These also include damped boundary conditions[20,46] and a momentum-space representation of the leads.[47] In the latter work, an interacting resonant level model has been studied with tDMRG and, effectively, a logarithmic discretization of the leads has been used. Working with different kind of leads, while preserving the main physical properties of the system, has thus proven to be a promising path that we will further pursue in this work.

It is the purpose of this paper to perform a numerical real-time analysis of Kondo correlations in quantum dot problems using tDMRG and Wilson chains. We show that, compared to a previous study by some of us,[20] a correct description of transport through a quantum dot can be obtained deeper into the Kondo regime, and using much smaller system sizes. While a tDMRG analysis of the Kondo regime based on a real-space description is hampered by finite-size effects in the leads, we show that an appropriate choice of hopping amplitudes in the leads nicely circumvents such problems.

In this sense, the discretization scheme proposed by Wilson is a natural choice: the noninteracting tight-binding chain becomes an effectively metallic system with reduced level spacings, corresponding to a subset of states directly coupled to the impurity in the continuum limit.[9,10] In addition, it turns out to offer advantages in the time-dependent description as well: for a given system size, it substantially increases the characteristic time scales over which a constant current flows between the leads, before reaching the system's boundary. This turns out to be crucial deeper into the Kondo regime (i.e., for small Kondo temperatures), as constant currents sustained over longer time scales are necessary to access the regime of coherent transport through the sharp, resonant Kondo state.[15,17,48] We also discuss and study the influence of the discretization at finite-bias. In the low-bias regime, the logarithmic discretization gives the correct description of the Kondo regime, at large bias, (where the Kondo effect is effectively destroyed), a linear discretization of the leads and larger chains should be used.

The paper is organized as follows: In Sec. II we introduce our approach, using the example of a single quantum-dot connected to metallic leads out of equilibrium, treated with the tDMRG method. Results for the time-dependent currents and charge transfer are discussed in Secs. III and IV, respectively. Particular emphasis is devoted to describing the improvements obtained by choosing a $\Lambda > 1$ model over the $\Lambda = 1$ case, and to the dependence of our results on both the discretization parameter and the system size. Moreover, we discuss the conductance results, taken from the time-dependent data, in Sec. V. In Sec. VI, we provide a discussion of how to approach the finite-bias regime by combining tDMRG data obtained from discretized and tight-binding leads. We present a summary in Sec. VII. Two appendices conclude this work: App. A contains our results for the noninteracting case, and App. B provides a discussion on the computational aspects of our approach and the entanglement growth during the time-evolution.

II. MODEL AND SET-UP

As a case study of the proposed modification of the method, we apply tDMRG to a model representing a single quantum dot connected to metallic leads. The equilibrium and linear-response properties of this system are well known and provide a natural benchmark against which we can compare the tDMRG results.

The quantum dot is modeled by a Hubbard site with an on-site interaction U and a gate potential V_g coupled to noninteracting tight-binding chains, representing the leads, as depicted in Fig. 1. The dot-lead couplings are labeled by t'. The full Hamiltonian reads $H = H_{\text{Dot}} + H_{\text{Dot-Leads}} + H_{\text{Leads}}$, with

$$\begin{aligned} H_{\text{Dot}} &= V_g \hat{n}_0 + U \hat{n}_{0\downarrow} \hat{n}_{0\uparrow} \,, \\ H_{\text{Dot-Leads}} &= -t' \sum_{\sigma,\alpha=R,L} \left(c^\dagger_{0,\sigma} c_{1,\alpha,\sigma} + \text{h.c.} \right) \,, \\ H_{\text{Leads}} &= - \sum_{\sigma,\alpha=R,L} \sum_{n=1}^{N_\alpha} t_n \left(c^\dagger_{n,\alpha,\sigma} c_{n+1,\alpha,\sigma} + \text{h.c.} \right) , \end{aligned} \tag{1}$$

where $c^\dagger_{n,\alpha,\sigma}$ creates an electron with spin σ at site n in lead α ($n = 0$ is the dot site), N_α counts the number of sites in lead α, and $\hat{n}_{i\sigma} = c^\dagger_{i,\sigma} c_{i,\sigma}$; $\hat{n}_i = \hat{n}_{i\uparrow} + \hat{n}_{i\downarrow}$ with $i = 0, \{n, \alpha\}$. The total number of sites is thus $N = N_L + 1 + N_R$. Our results were obtained using "even-1-odd" chains, with $N_L = N/2$, $N_R = N/2 - 1$. Note that finite-size effects due to different cluster types, as discussed in Ref. 49, vanish at sufficiently large Λ.

In the spirit of Wilson's discretization scheme, we consider the hopping matrix elements t_n in the leads to decay

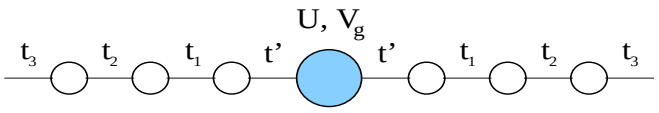


FIG. 1: (color online) Schematic representation of the model describing a quantum dot (large circle, blue in the online version) connected to left and right leads.

exponentially as

$$t_n = t_0\,\Lambda^{-n/2}\,, \tag{2}$$

where $\Lambda \geq 1$ is the "discretization parameter" from Wilson's original formulation.

Unless otherwise noted, in the following we set $t_0 = 1$, $U = 1$, $V_g = -U/2$ (particle-hole symmetric point). We focus on results for $N = 32$ sites for $\Lambda > 1$ and up to $N = 128$ sites for $\Lambda = 1$. We usually work at half-filling of the whole system. In the range of parameters considered, the equilibrium ground-state properties for $\Lambda > 1$ do not change significantly upon increasing N beyond a certain $N^*(\Lambda) < 50$ at a given Λ, as we have numerically verified for a few cases. This is consistent with NRG runs for an Anderson model with similar parameters, which reach the Kondo fixed point with less than 50 iterations for $\Lambda \sim 2 - 3$.

Details on the tDMRG can be found in Refs. 37,38. We use a Trotter–Suzuki breakup of the time-evolution operator and typical time steps of $\delta\tau = 0.01$–0.1. A larger time-step $\delta\tau \sim 0.4$ is sufficient when deeper in the Kondo regime (large U/t'^2) as resonant transport is dominated by a small energy scale, the Kondo temperature, corresponding to long time scales.[17,48] Note that we denote time by the symbol τ and it is measured in units of $\hbar/t_0$. The truncated weight $\delta\rho$ during the time-evolution is typically kept below 10^{-7} (see App. B for a discussion).

In order to drive a current, we first compute the ground state of the system without a bias. The bias is applied as

$$H_{\rm bias} = \frac{\Delta V}{2}\sum_{n=1}^{N_R}\hat{n}_{R,n} - \frac{\Delta V}{2}\sum_{n=1}^{N_L}\hat{n}_{L,n} \tag{3}$$

in the leads at time τ and we then evolve in time under the dynamics of $H + H_{\rm bias}$. We typically work at a small bias of $\Delta V = 0.005$ (the finite-bias case is discussed in Sec. VI). The current $J(\tau)$ is measured as the average over the expectation values of the local current operator

$$\hat{J}_{1,\alpha} = it'\sum_{\sigma}(c^\dagger_{0,\sigma}c_{1,\alpha,\sigma} - \text{h.c.}), \tag{4}$$

on the links connecting the dot to the leads. This means that we first take its expectation value in the time-dependent wave-function and then average over the two local currents on the links directly connected to the dot. We have tried other spatial forms for the applied bias, *e.g.*, a broadened step function.[38] This mostly affects the short-time transient behavior, but leaves unaffected the average value of the current taken over time (see Sec. V). Further details on the set-up can be found in Ref. 20.

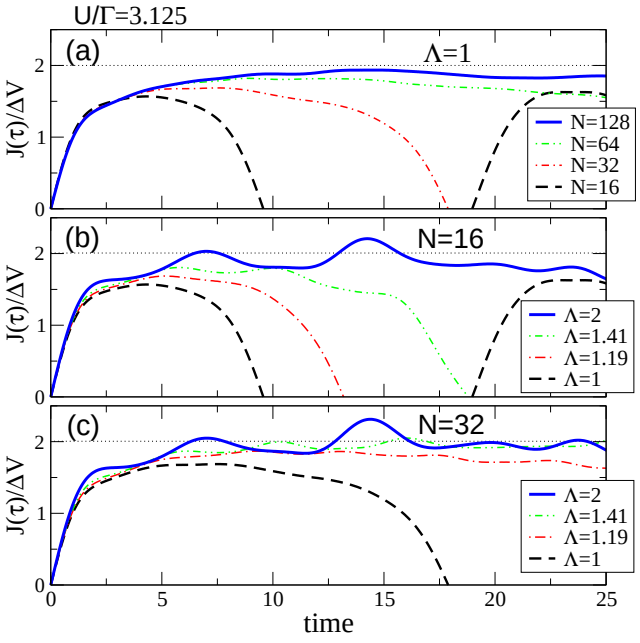


FIG. 2: (color online) Conductance $J(\tau)/\Delta V$ for $U = 1$, $t' = 0.4$, $V_g = -U/2$. (a) Fixed $\Lambda(= 1)$, and $N = 16$, 32, 64 and 128; (b),(c): Fixed N. (b) $N = 16$ and (c) $N = 32$ with $\Lambda = 1$, $2^{1/4}$, $\sqrt{2}$, and 2.

III. TIME-DEPENDENT CURRENTS

Figure 2 shows the current $J(\tau)$ (in units of e^2/h) as a function of time and divided by the external bias ΔV, at $U = 1$, $t' = 0.4$. This corresponds to a ratio of $U/\Gamma = 3.125$, where $\Gamma = \pi\rho_{\rm leads}(t')^2$ is the hybridization parameter and $\rho_{\rm leads} = 2/(\pi t_0)$ is the density of states of the leads in the limit of $\Lambda = 1$ and long chains.

Figure 2(a) contains the results for $N = 16, 32, 64, 128$ at $\Lambda = 1$, reproducing those of Ref. 20. The other two panels display $J(\tau)/\Delta V$ for (b) $N = 16$ and (c) $N = 32$, computed with $\Lambda = 1, 2^{1/4}, \sqrt{2}$, and 2.

The comparison between Fig. 2(a) and (c) is revealing. In the $\Lambda = 1$ case, the conductance plateaus become longer and higher as the system size increases[20] with the "plateau length" ($\equiv \tau_{\rm st}$) increasing linearly with N. For $N = 128$ sites, a nearly perfect conductance plateau with $G(\tau) \approx G_0$ is obtained for these parameters. A finite-size scaling analysis, done in Ref. 20 for $U/\Gamma = 3.125$, shows that $G \to G_0$ for $N^{-1} \to 0$.

As previously argued in Ref. 20, this plateau signals the formation of a Kondo state in the system formed by the quantum dot and the leads. A similar Kondo conductance plateau can be obtained by increasing Λ while keeping the system size *constant*, as shown in Figs. 2(b) and

(c). Interestingly, for $N = 32$, a plateau with an average conductance of $G \approx G_0$ can be obtained with $\Lambda = 2$. Thus, an accurate description of the Kondo regime can be obtained using a relatively small system by taking $\Lambda > 1$.

Notice that the $J(\tau)/\Delta V$ curve for $\Lambda = 2$ and $N = 32$ is similar to the corresponding one for $N = 16$: an increase in system size had little effect in the current in this case, as opposed to the $\Lambda = 1$ curves. This weak dependence of $J(\tau)$ on N for large enough N and Λ is a general feature of the $\Lambda > 1$ case, and it is a consequence of the exponential decrease of the hopping matrix elements t_n at large n.

This allows us to formulate some key results that can be inferred from this plot: (i) By comparison of Fig. 2 (a) and Fig. 2 (c), we find that with discretized leads, a four times smaller system size is sufficient to obtain roughly the same average current. (ii) At $\Lambda > 1$ and for a given N, the current plateaus are longer in time and, on the time-scales simulated, we do not observe a recurrence (bouncing current) in the case of $N = 32$. (iii) Oscillations about the average value of the current tend to increase with Λ.

The small time-scale oscillations are a general feature of the $\Lambda > 1$ case, which emerges in the $U = 0$ case as well, as we have verified with exact diagonalization (see App. A). We have conducted extensive checks to rule out either the truncation error during the time evolution or the size of the time-step as possible sources of such oscillations at finite U. In fact, the position of the peaks and valleys of the oscillations as seen in Figs. 2(b) and (c) are Λ-dependent: for a given Λ, the position of these peaks and valleys remains practically constant even when other parameters, such as t' or V_g, are modified, while it changes as Λ is varied (see App. A).

The oscillations are reminiscent of the so called "current ringing" in mesoscopic transport.[15] Similar current ringing effects have been observed in previous tDMRG studies of noninteracting systems away from half-filling or at finite bias.[21,38,50] In the present case of both a finite U and $\Lambda > 1$, the oscillations are present even at half-filling and become more prominent at larger values of Λ. We stress that the oscillations seen in the $\Lambda > 1$ case are an artefact of the discretization and are thus not a property of the $\Lambda \to 1$, $N \to \infty$ limit. In practice, the oscillations can be reduced by using the so-called z-trick,[11,51,52] which we illustrate in App. A for the noninteracting case.

We attribute the increase of the average current on small chains at larger Λ to a combination of mainly two factors: (i) an effective reduction in the mean-level spacing in the leads in equilibrium and, quite importantly, (ii) an increase in the duration of the non-equilibrium current plateaus above a characteristic Kondo time scale. As the exponential decay of hoppings leads to an exponential decrease in the velocity at which charges move far away from the dot, those charges get trapped at the leads and a recurrence, *i.e.*, a reversal of the current's sign, is not observed. We will elaborate on this point in the following section.

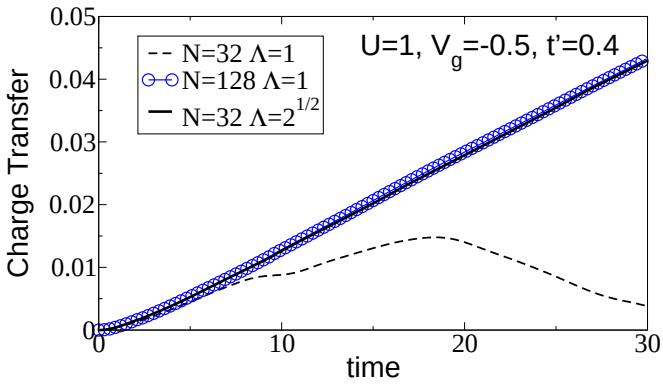


FIG. 3: (color online) Charge transfer for $\Lambda = 1$, $N = 32$ (dashed lines), $\Lambda = 1$, $N = 128$ (open circles) and $\Lambda = \sqrt{2}$, $N = 32$ (solid line). The parameters are $U = 1$, $V_g = -U/2$, and $t' = 0.4$ ($U/\Gamma = 3.125$). The maximum in the charge transfer for $N = 32, \Lambda = 1$ indicates a reversal in the current.

Before turning to the calculation of conductances from our time-dependent data, we will discuss the charge profiles and charge transfer during the time-evolution.

IV. CHARGE PROFILE AND CHARGE TRANSFER

Since no dissipative terms are included in the Hamiltonian (1), the total charge is conserved at all times. Thus, the existence of a net current signals the transfer of charge from one lead to the other. As time progresses, a saturation point might be reached, opening the possibility for the current to decrease and reverse sign, and to transfer the excess charge back to the original lead.[20,21]

This mechanism is shown, for instance, in Fig. 2(a) ($\Lambda = 1$): for $N = 16$ the current reverses sign around $\tau = 9$ while for $N = 32$ the sign reversal occurs at $\tau = 18$. Such sign reversal also occurs for $N = 128$ and $\Lambda = 1$, at times $\tau \gg 25$.

Figure 3 shows the *charge transfer* into the left lead (l), defined as ($n_i(\tau) = \langle \hat{n}_i(\tau) \rangle$):

$$\Delta n_{\rm L}(\tau) = \sum_{i \in {\rm L}} [n_i(\tau) - n_i(0)] \, . \qquad (5)$$

Notice that this quantity is related to the time-integrated current through the dot: it hence reaches a maximum whenever the current changes sign. For $\Lambda = 1$ and $N = 32$, $\Delta n_l(\tau)$ reaches a maximum ($\Delta n_{l,\max} \approx 0.01$) at $\tau = 18$ while for $\Lambda = \sqrt{2}$, it increases to about four times that value. Remarkably, in order to obtain a similar charge transfer enhancement with "regular" leads ($\Lambda = 1$), a four-fold increase in the system size is needed (open circles in Fig. 3).

The approximately linear increase in $\Delta n_l(\tau)$ is correlated with the plateau in the current in both cases (compare with Fig. 2). We identify this as a general feature

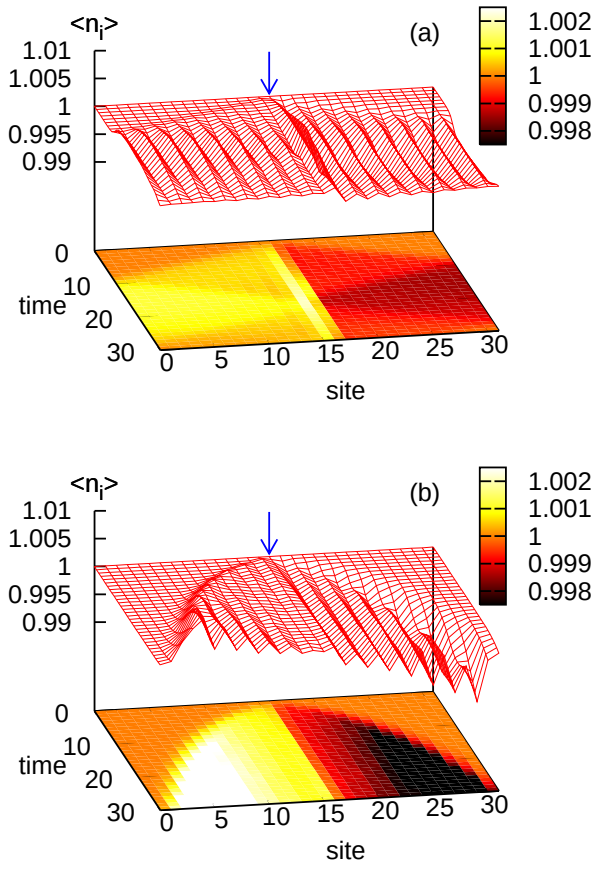


FIG. 4: (color online) Charge profile of the 16-1-15 chain (single dot), $V_g = -U/2$: (a) $\Lambda = 1$ and (b) $\Lambda = \sqrt{2}$. The dot site is indicated by arrows in both plots.

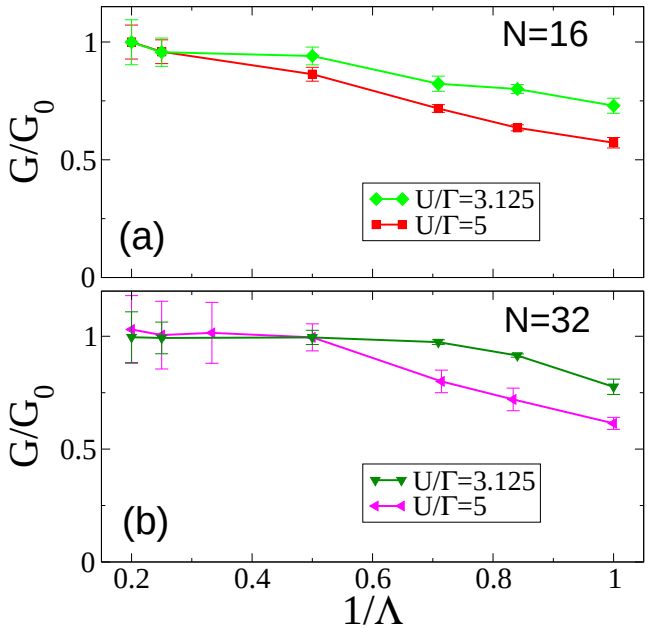


FIG. 5: (color online) Scaling with $1/\Lambda$ of the conductance G for (a) $N = 16$ and (b) $N = 32$, $V_g = -U/2$, and different values of U/Γ.

of the introduction of the decaying hopping matrix elements for a given system size N: an enhanced charge transfer over longer time scales.

This indicates that the exponential decay in the hoppings increases the maximum charge that can be "stored" in the leads, or, in other words, it provides an increase in their effective "capacitance". As a consequence, even small systems can hold a larger amount of charge without reversing the current, leading to longer constant-current plateaus.

The effect of $\Lambda > 1$ can be illustrated by considering the time evolution of the charge profile. Figure 4 shows the charge $n_l(\tau)$ on each site l of the chain plotted against time for a chain of $N = 32$ sites. The top panel shows the $\Lambda = 1$ case: charge is initially transferred from the left to the right lead and back, leading to an oscillation in $n_l(\tau)$ with a maximum around $\tau = 18$, as expected. The charge versus time diagram clearly shows a light-cone with a wave-front that propagates at the Fermi velocity. Notice that the excess charge is mostly accumulated in the vicinity of the dot, which we expect to modify the leads' density of states "seen" by the dot.

This is in sharp contrast with the $\Lambda = \sqrt{2}$ case (bottom panel): a larger charge is transferred to the left lead and no reflux is noticed. More importantly, the charge tends to accumulate toward the edge of the leads, with strong Friedel oscillations. This can be intuitively understood from the exponential decrease in the couplings: the weak coupling of the end sites with the remaining of the chain makes them good "charge traps".

V. THE CONDUCTANCE

We now turn to the linear conductance $G(\tau) \equiv J(\tau)/\Delta V$, expressed in units of $G_0 \equiv 2e^2/h$. We will discuss the dependence of $G(\tau)$ on Λ and N, at the particle-hole symmetric point. For this purpose, we refer the reader back to Fig. 2. Taking the example of $\Lambda = 2$, we see that no significant difference exists between the conductance curves for $N = 16$ and $N = 32$. In general, for a given Λ there exists a certain system size above which no significant changes in properties, such as the ground state energy or the conductance, take place as extra sites are added to the system.

In order to study the dependence of the conductance with other parameters, we calculate the *average conductance* $G = \langle G(\tau) \rangle_\tau$ over a plateau, *e.g.*, those displayed in Fig. 2. This procedure carries an intrinsic uncertainty which depends on the truncated weight in the DMRG time evolution and, more importantly, on the dispersion of $G(\tau)$ around the average due to the current ringing effects at larger Λ. While the former can be constrained below a target value by increasing the number of states

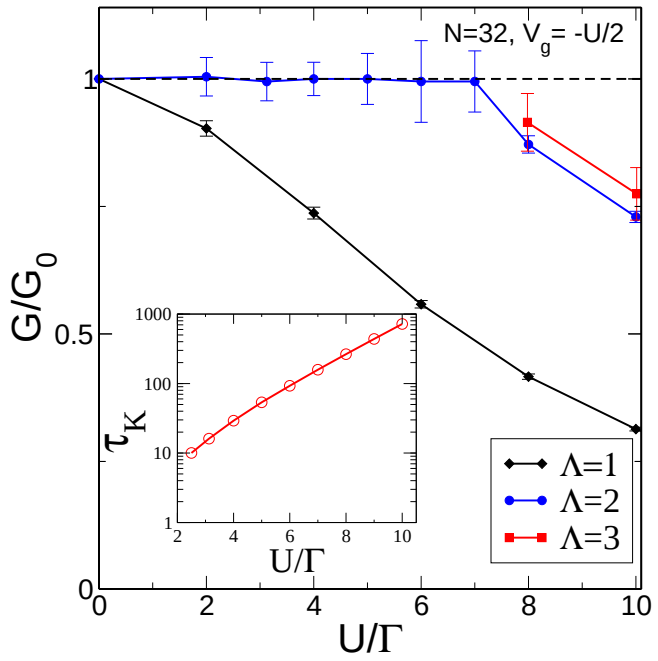


FIG. 6: (color online) Average conductance $G \equiv \langle G \rangle_\tau$ vs. U/Γ for $\Lambda = 1, 2$ and 3, and N=32 (dashed line is a guide to the eye). For $\Lambda > 1$, the averages are taken over time intervals $\tau_K \lesssim \tau \lesssim \tau_{\max}$. For $U/\Gamma \leq 7$, maximum simulation times are $\tau_{\max} \approx \tau_K + 100$. For $U/\Gamma \gtrsim 8$ (included for illustration), $\tau_K > \tau_{\max}$, hence $G < G_0$. Inset: Kondo time τ_K (calculated with NRG) vs. U/Γ. See the text for details.

that are kept during the time evolution (see the discussion in App. B), the latter is intrinsic for $\Lambda > 1$. We estimate such uncertainty by computing

$$\delta G = \sqrt{\langle G(\tau)^2 \rangle_\tau - \langle G(\tau) \rangle_\tau^2}, \tag{6}$$

and indicate it as error bars in the figures. We remark that the main contribution to δG in the plots comes from the current-ringing oscillations (see the analysis in App. A).

Figures 5(a) and (b) show the scaling of $G \equiv \langle G(\tau) \rangle_\tau$ with $1/\Lambda$ for different values of U/Γ, and for $N = 16$ and 32, respectively. The scaling is more conclusive for $N = 32$: $G \to G_0$ as $1/\Lambda$ decreases, for $U/\Gamma \lesssim 5$. Most importantly, Fig. 5(b) establishes the convergence of the conductance in $1/\Lambda$ (obtained at a fixed system size) to the correct result, namely perfect conductance.

Figure 6 depicts results for G/G_0 as a function of U/Γ, for $N = 32$, $\Delta V = 0.005$, and $\Lambda = 1$, 2, and 3. With $\Lambda > 1$, we obtain perfect conductance up to $U/\Gamma \approx 7$. This constitutes a considerable improvement over the $\Lambda = 1$ case with $N = 32$ (also shown in Fig. 6), for which perfect conductance plateaus were not observed for nonzero U/Γ. Furthermore, we stress that the $\Lambda > 1$ approach also gives more well defined plateaus of constant currents, which in practice makes easier the averaging of $J(\tau)/\Delta V$ over time.

The improvement previously discussed is anchored on a combination of two key elements in the $\Lambda > 1$ case: (i) an effective reduction in the level spacing of the metallic leads in equilibrium[44] and (ii) the suppression of the current reversal, which is a consequence of the reduced velocity in the leads when $\Lambda > 1$. Both points are related to the exponential decrease in the chain hoppings, which, in Wilson's scheme, can be traced back to a representation of the continuum of states directly connected to the quantum dot.

Point (ii) is important for the following reason: in resonant transport, the typical time scale for reaching the steady state is inversely proportional to the width of the resonance.[15,21] The typical time scale associated with the development of the perfect conductance plateaus associated with the Kondo state is thus $\tau_K \equiv \hbar/T_K$.[17,48] It is then crucial that the current does not reverse sign before times of order τ_K have been reached.

As explained in Sec. III, for $\Lambda = 1$ the plateaus last over time intervals $\tau_{\rm st} \propto N$ and a compromise must be obtained between T_K and N such that the condition $\tau_{\rm st} \gtrsim \tau_K$ is fulfilled. For $\Lambda > 1$, this condition can be met by increasing Λ (instead of N), since $\tau_{\rm st}$ increases with Λ, as discussed in Sec. III. Constant currents corresponding to perfect conductance can, in principle, be reached for Λ values large enough so that $\tau_{\rm st}(\Lambda) > \tau_K$. In this sense, this requirement marks the regime for which the steady state of this problem can be numerically simulated.

Once the condition $\tau_{\rm st}(\Lambda) > \tau_K$ is fulfilled, one still needs to run the tDMRG algorithm over time scales of order τ_K to obtain the Kondo plateau. Thus, for higher values of U/Γ (*i.e.*, higher τ_K), calculations over longer time scales are necessary in order to reach nearly perfect conductance plateaus in $J(\tau)$.[15] This is, due to the entanglement growth in a global quench,[53,54] the true limitation of the method for Kondo problems. Fortunately, the entanglement growth turns out to be softer at large values of U/Γ (see App. B), enabling us to observe $G \approx G_0$ for up to $U/\Gamma \sim 6$ and relatively short ($N = 32$) chains.

This argument is further supported by quantitative estimates for τ_K obtained with NRG (inset in Fig. 6). We performed NRG calculations for the Anderson model and extracted the Kondo temperature (and thus τ_K) from the magnetic susceptibility curves for different values of U/Γ.[55] For the parameters in Fig. 6, we obtain $\tau_K < \tau_{\rm st}$ in the regime where nearly perfect conductance is seen in the tDMRG curves ($\tau_K \simeq 16$ for $U/\Gamma = 3.125$ and $\tau_K \simeq 55$ for $U/\Gamma = 5$, in units of $\hbar/t_0$).[56] For higher values of U/Γ, τ_K becomes exponentially large. In particular, for $U/\Gamma \sim 7$, τ_K calculated from NRG becomes of the order of the maximum time scales used in our tDMRG simulations. This explains the noticeable deviation of G from the Kondo value for $U/\Gamma > 7$.

In short, the tDMRG results obtained with $\Lambda > 1$ constitute a considerable improvement over the $\Lambda = 1$ case, as shown in Fig. 6 for $N = 32$. This plot illustrates the range of parameters for which the Kondo regime is accessible with tDMRG and $\Lambda > 1$, as well as the typical system sizes.

VI. FINITE BIAS

In this Section, we address the case of a current through a quantum dot in the Kondo regime driven by a finite bias. Although a comprehensive theoretical understanding of this nonequilibrium regime is yet to be achieved, one commonly expects the applied bias ΔV to disrupt the Kondo state for bias voltages larger than T_K while Kondo-like properties are only marginally affected for $\Delta V \ll T_K$.[25,29,30,31] We investigate the transport properties of the system in these two regimes. In the following, we fix the parameters to $U/\Gamma = 3.125$ at the particle-hole symmetric point ($V_g = -U/2$), for which we have independently determined T_K from NRG calculations[56] (see the inset in Fig. 6).

Qualitatively, we expect the linear regime (i.e., nearly perfect conductance) to extend up to biases $\Delta V \sim T_K$. The current versus bias curve should then smoothly drop to zero at larger biases. We argue that, in the spirit of the previous sections, in the regime $\Delta V < T_K$, the finite-bias regime should best be explored with discretized leads, for which the Kondo state is better described.

By contrast, in the opposite limit of $\Delta V \gg T_K$, the scan in bias will need the high-energy features (such as the band curvature in the leads) to be well resolved as the contribution to the current from states with energies within the Fermi levels in the left and the right leads becomes important. Therefore, at $\Delta V \gg T_K$, the best approach is to use $\Lambda = 1$ in the tDMRG calculations and subsequently perform a finite-size scaling analysis of the average currents.

Our results are illustrated in Fig. 7. Fig. 7(a) shows the current versus time for different bias values and $\Lambda = 1$, $N = 72$ and $\Lambda = 2$, $N = 32$. As a general feature, the average current $\langle J\rangle_\tau$ increases with the bias ΔV in all cases, also seen in Fig. 7(b). Moreover, it is evident that for the values of ΔV depicted in Fig. 7(a), runs with either $\Lambda = 1$ or $\Lambda = 2$ give a *qualitatively* similar behavior.

A more quantitative analysis of the $\langle J\rangle_\tau(\Delta V)$ curves obtained from the tDMRG data is presented in Figs. 7(b) and 7(c). Deviations from perfect conductance ($\langle J\rangle_\tau = G_0\Delta V$) are clear at large bias (Fig. 7(b)). At small biases, the results are better visualized by numerically calculating the differential conductance $d\langle J\rangle_\tau/d(\Delta V)$, shown in Fig. 7(c). For small ΔV, this quantity is equivalent to the linear conductance.

For $\Lambda = 1$ and $N = 72$ sites, we see that the corresponding $d\langle J\rangle_\tau/d(\Delta V)$ curve is substantially below G_0 for $\Delta V \lesssim T_K$ in sharp contrast with the $\Lambda = 2$ results, emphasizing the importance of using Wilson chains at small biases. At large biases, we have performed a finite-size scaling analysis with $N \leq 80$, and we conclude that the data displayed in Fig. 7(c) are converged down to $\Delta V \gtrsim 0.15$ with an uncertainty of $\delta\left[d\langle J\rangle_\tau/d(\Delta V)\right] \sim 0.01$.

In an intermediate bias regime of $T_K \lesssim \Delta V \lesssim 0.15$, the $\Lambda = 1$ results are still plagued by finite-size effects,

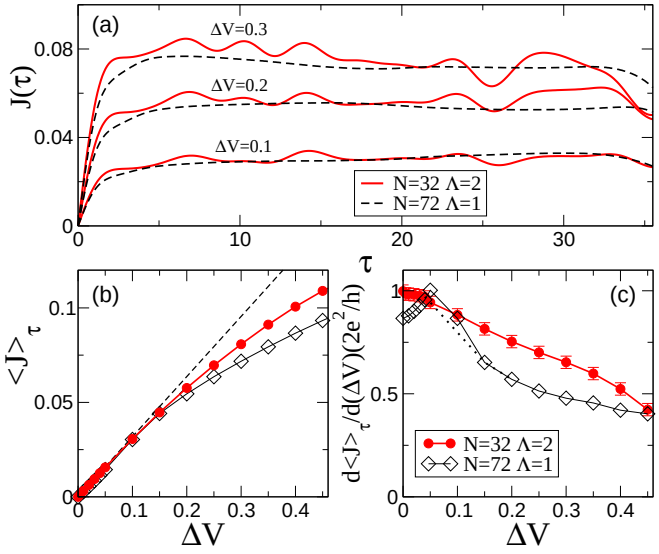


FIG. 7: (color online) (a) Current $J(\tau)$ versus time for $\Delta V = 0.1, 0.2, 0.3$ and $\Lambda = 1$ ($N = 72$) and $\Lambda = 2$ ($N = 32$). (b) Average current $\langle J\rangle_\tau$ and conductance $d\langle J\rangle_\tau/d(\Delta V)$ as a function of bias. The dashed line is $\langle J\rangle_\tau = G_0\Delta V$. (c) Differential conductance for $\Lambda = 1$ ($N = 72$) and $\Lambda = 2$ ($N = 32$). The dotted line represents an interpolation between the low bias regime (better described by $\Lambda = 2$) and the high bias one (better described by $\Lambda = 1$).

while the $\Lambda = 2$ results overestimate the actual steady-state currents. In this regime, a discretization scheme that interpolates between linear and a logarithmic discretization will likely be the best choice. Qualitatively, one can estimate the expected result by a linear interpolation between the $\Lambda = 1$ and $\Lambda > 1$ data, as illustrated by the dotted line in Fig. 7(c)

Finally, note that the finite-bias regime of a single-impurity Anderson model has been studied with tDMRG by Kirino *et al.* (Ref. 25) for $U/\Gamma \lesssim 2.8$ and system sizes of up to $N = 64$ (all at $\Lambda = 1$). Here, we slightly exceed that regime by working at $U/\Gamma = 3.125$, and we also consider larger system sizes of $N = 64, 72, 80$. Our key point, though, is that tDMRG runs at $\Delta V \lesssim T_K$ notoriously improve and correctly capture Kondo correlations when performed with Wilson chains .

VII. SUMMARY

In this paper, we applied the tDMRG method to the study of transport through a quantum dot coupled to noninteracting leads with a logarithmic discretization. This yields a considerable improvement over tDMRG studies with real-space tight-binding leads, as it extends the parameter space in which known exact results can be reproduced. One of the main advantages of the approach is that smaller chains are sufficient to obtain the expected result of a perfect conductance for the single-impurity problem at particle-hole symmetry.

In spite of the challenges imposed by the longer time scales needed for the description of the Kondo regime, the study of transport properties in nanostructures with time-dependent DMRG brings several advantages over other methods: it is straightforward to adapt codes to more complicated geometries and time-dependent Hamiltonians, including correlation effects in the leads, as well as systems far from equilibrium, such as transport beyond the linear response regime (finite-bias).[25] For the latter example, we presented a case study at an intermediate U/Γ to argue that for bias values ($\Delta V \lesssim T_K$), a logarithmic discretization should preferentially be used, while at large bias, a regime in which high-energy features of the leads dominate, a tDMRG study with $\Lambda = 1$ and a finite-size scaling analysis yields better results.

Furthermore, we believe the general concept of utilizing a logarithmic discretization in tDMRG can have a broader range of applicability in the description of Kondo systems. In particular, it can play a key role in the calculation of nonequilibrium dynamic correlation functions, as recently highlighted in NRG-based approaches.[24]

Acknowledgments

We sincerely thank K. A. Al-Hassanieh, I. P. McCulloch, G. Roux, H. Onishi, and U. Schollwöck for fruitful discussions and valuable comments on the manuscript. Research at ORNL is sponsored by the Division of Materials Sciences and Engineering, Office of Basic Energy Sciences, U.S. Department of Energy, under contract DE-AC05-00OR22725 with Oak Ridge National Laboratory, managed and operated by UT-Battelle, LLC. E.D., and L.D.d.S. are supported in part by NSF grant DMR-0706020. F.H.-M. acknowledges support from the DFG through FOR 912. G.B.M. and C.A.B. acknowledge support from NSF (DMR-0710529). E.V.A. acknowledges support from Brazilian agencies FAPERJ and CNPq (CIAM 490865/2006-2)

APPENDIX A: NONINTERACTING CASE

In this appendix, we present exact diagonalization results for the time-dependence of the current Eq. (4) for a chain of $N = 32$ sites and $t' = 0.4$. Figure 8 shows $J(\tau)$ vs. time for $\Lambda = 1, 1.4, 2$. Some main features induced by the discretization discussed in Sec. III are already present in the noninteracting case: (i) as Λ is increased, the sign reversal of the current occurs at much later times and (ii) while the average current in the $U = 0$ case remains at $G = G_0$, the dispersion around this mean value is significantly enhanced by a $\Lambda > 1$.

More specifically, by taking averages over suitable time intervals, we find $G/G_0 = (1.00 \pm 0.04)$ and $G/G_0 = (1.00 \pm 0.13)$, for $\Lambda = 1.4$ and 2, respectivley. The deviations are computed from Eq. (6). We thus conclude that

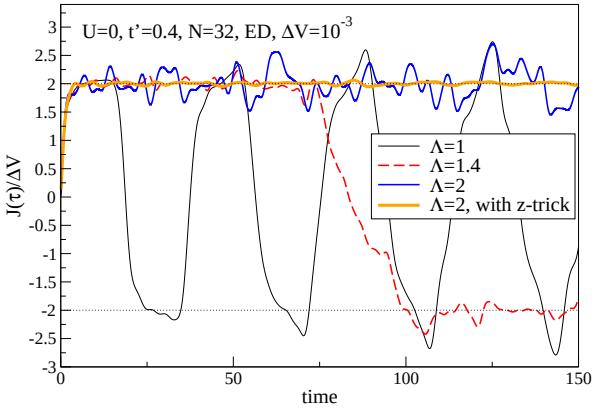


FIG. 8: (color online) Current $J(\tau)$ as a function of time for the noninteracting case ($U = 0$, $V_g = 0$, $t' = 0.4$, $N = 32$) for different values of $\Lambda = 1, 1.4, 2$, calculated with exact diagonalization.

the oscillations seen in Fig. 2 in the interacting case are due to the discretization.

Moreover, from the noninteracting case we learn that using the logarithmic discretization, one manages to reproduce the average quite well. Once one has achieved that in the interacting case for a pair of (N, Λ), we expect that the oscillations will be reduced by increasing N and decreasing Λ at the same time in a controlled way such that the average current $J(\tau)$ remains constant.

An alternative way of suppressing the oscillations induced by the discretization is to exploit the so-called z-trick.[11,51,52] Indeed, this works quite well: the thick solid line in Fig. 8 is obtained by using the z-trick for $\Lambda = 2$, which clearly improves the data quality over the simple $\Lambda = 2$ curve. However, it turns out to be necessary to average over many values of z: results shown in Fig. 8 were obtained by averaging over forty $J(\tau)$-curves with z-values ranging from 0 to 1. In practice, this makes this procedure numerically expensive for tDMRG calculations.

APPENDIX B: COMPUTATIONAL ASPECTS

As a key result of this work, we have argued that using the logarithmic discretization much smaller chains than in the $\Lambda = 1$ case can be used to obtain equally good, if not better, results for the conductance. This suggests a gain in the computational costs needed to obtain the numerical results, by reducing the required system sizes roughly by a factor 4.

For a more stringent estimate of the computational efficiency, we consider the entanglement growth during the time-evolution. We measure this quantity by computing the *block entropy* S_l, associated with the reduced density matrix ρ_l of a DMRG block of length l:

$$S_l = -\langle \rho_l \ln \rho_l \rangle \,. \tag{B1}$$

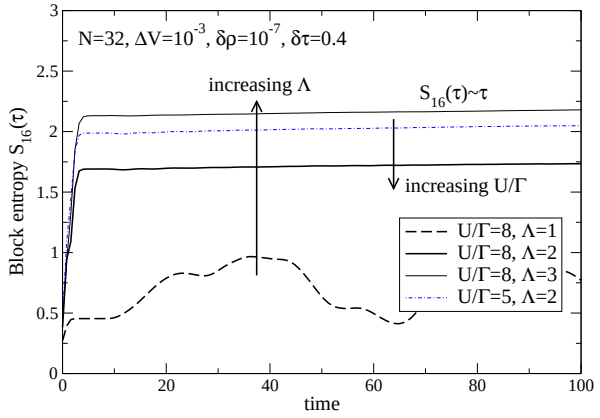


FIG. 9: (color online) Block entropy S_l for a block of length $l = 16$ vs. time for $U/\Gamma = 5$ ($\Lambda = 2$) and $U/\Gamma = 8$ ($\Lambda = 1, 2, 3$). $N = 32$ and $\Delta V = 10^{-3}$, the time steps $\delta\tau$, and the truncated weight $\delta\rho$ are given in the legend.

The reduced density matrix ρ_l is obtained at each step by dividing the DMRG chain (the so-called super-block) into "system" (size l) and "environment" parts, and tracing out the environment's degrees of freedom (see, *e.g.*, Ref. 35 for a discussion of the DMRG method). An increase in S_l renders a simulation inefficient as time or system size grows, since more DMRG states need to be kept in order to keep the truncation error below a given threshold.

In Fig. 9, we plot the block entropy for a block of length $l = 16$ as a function of time, for two different values of $U/\Gamma = 5$ ($\Lambda = 1$) and 8 ($\Lambda = 1, 2, 3$). Typically, the entropy rapidly increases at short times, but at times $\tau \gtrsim 3$, it exhibits a linear increase in time for $\Lambda > 1$, $S_l \propto \tau$. This is the expected behavior for a global quench,[53,54,57] yet it is a non-obvious one here as the excitations in the leads do not travel at a constant velocity (see Fig. 4(b)). The oscillations in $S_l(\tau)$ seen in the $\Lambda = 1$ case (dotted line) are due to the sign reversal of the current. The key point is that this linear increase is slow, *i.e.*, the prefactor is small. During the time interval $\tau \in [5, 100]$, S_l only grows by a few per cent. This is ultimately the reason why we can push our tDMRG runs to times long enough to reach the steady state for $U/\Gamma \lesssim 6$ at moderate numerical costs, especially since the entanglement growth is the weaker the larger U/Γ is.

We thus observe that the entanglement growth, *i.e.*, the increase in the entropy S_l, depends on both Λ and U/Γ. Yet, it is fortunate that in the case where longer times are needed in order to capture the steady-state current (large U/Γ) the increase in S_l is weaker.

It is illustrative to give an example on what the entanglement growth implies in practice for the numerical effort when working at a fixed truncation error $\delta\rho$. For $U/\Gamma = 3.125$, we find it sufficient to keep $m \sim 280$ states at $\Lambda = 1$ in order to ensure a maximum truncated weight of $\delta\rho \sim 10^{-7}$ on a chain of $N = 32$ sites, compared to $m \sim 1000$ at $\Lambda = \sqrt{2}$ and $m \sim 1600$ at $\Lambda = 3$ (both numbers refer to times $\tau \lesssim 30$ with $\delta\tau = 0.05$). At a larger U/Γ, say 12.5, this relaxes to $m \sim 200$ and $m \sim 400$, for $\Lambda = 1$ and $\Lambda = \sqrt{2}$, respectively.

We finally comment on the generic tDMRG errors, the accumulated truncation error, and the Trotter error. These are not independent: the smaller the time step, the faster truncation errors will accumulate.[58] We justify our choice of parameters by considering the numerically worst case, *i.e.*, a small $U/\Gamma \sim 3$.

For most calculations, keeping a maximum of $m = 660$ states up to times of order $\tau \sim 50$ is sufficient to keep the truncation error below 10^{-7} ($\sim 3 \times 10^{-7}$ in a few sweeps). More importantly, we have checked that, keeping up to $m = 1600$ states, the current $J(\tau)$ is practically converged: for the case of Fig. 2(c) and $\Lambda = 2$, the maximum relative change in $J(\tau)$ is $\sim 1\%$, comparing runs with $\delta\rho = 10^{-7}$ and $\delta\rho = 10^{-8}$. In addition, we have calculated the forth-back error[58] to validate that this is a sufficiently small discarded weight for our purposes, in which the oscillations cause the dominant fluctuation around the current's average (see App. A).

We have further checked our tDMRG with the chosen parameters against exact diagonalization for the noninteracting case to make sure that the so-called run-away time[58] is not the limiting factor in our case.

[1] C. Joachim, J. Gimzewski, and A. Aviram, Nature **408**, 541 (2000).
[2] D. Goldhaber-Gordon, H. Shtrikman, D. Mahalu, D. Abusch-Magder, U. Meirav, and M. A. Kastner, Nature **391**, 156 (1998).
[3] W. G. van der Wiel, S. D. Franceschi, T. Fujisawa, J. M. Elzerman, S. Tarucha, and L. P. Kouwenhoven, Science **289**, 2105 (2000).
[4] J. Park, A. N. Pasupathy, J. I. Goldsmith, C. Chang, Y. Yaish, J. R. Petta, M. Rinkoski, J. P. Sethna, H. D. Abruna, P. L. McEuen, and D. C. Ralph, Nature **417**, 722 (2002).
[5] P. Jarillo-Herrero, J. Kong, H. S. van der Zant, C. Dekker, L. P. Kouwenhoven, and S. D. Franceschi, Nature **434**, 484 (2005).
[6] A. Makarovski, J. Liu, and G. Finkelstein, Phys. Rev. Lett. **99**, 066801 (2007).
[7] R. M. Potok, I. G. Rau, H. Shtrikman, Y. Oreg, and D. Goldhaber-Gordon, Nature **68**, 05556 (2007).
[8] G. D. Mahan, *Many-Particle Physics*, Plenum Press, New York London, 1990.
[9] A. Hewson, *The Kondo Problem to Heavy Fermions*, Cambridge, UK, 1993.
[10] K. G. Wilson, Rev. Mod. Phys. **55**, 583 (1983).
[11] R. Bulla, T. Costi, and T. Pruschke, Rev. Mod. Phys. **80**, 395 (2008).
[12] W. B. Thimm, J. Kroha, and J. von Delft, Phys. Rev. Lett. **82**, 2143 (1999).

[13] I. Affleck and P. Simon, Phys. Rev. Lett. **86**, 2854 (2001).
[14] T. Hand, J. Kroha, and H. Monien, Phys. Rev. Lett. **97**, 136604 (2006).
[15] N. S. Wingreen, A.-P. Jauho, and Y. Meir, Phys. Rev. B **48**, 8487 (1993).
[16] H. Schoeller and J. König, Phys. Rev. Lett. **84**, 3686 (2000).
[17] A. Schiller and S. Hershfield, Phys. Rev. B **62**, R16271 (2000).
[18] A. Rosch, J. Kroha, and P. Wölfle, Phys. Rev. Lett. **87**, 156802 (2001).
[19] S. Kehrein, Phys. Rev. Lett. **95**, 056602 (2005).
[20] K. A. Al-Hassanieh, A. E. Feiguin, J. A. Riera, C. A. Büsser, and E. Dagotto, Phys. Rev. B **73**, 195304 (2006).
[21] G. Schneider and P. Schmitteckert, cond-mat/0601389 (unpublished).
[22] F. B. Anders and A. Schiller, Phys. Rev. Lett. **95**, 196801 (2005).
[23] F. B. Anders, Phys. Rev. Lett. **101**, 066804 (2008).
[24] F. B. Anders, arXiv:0803.3004 (unpublished).
[25] S. Kirino, T. Fujii, J. Zhao, and K. Ueda, J. Phys. Soc. Jpn. **77**, 084704 (2008).
[26] B. Doyon and N. Andrei, Phys. Rev. B **73**, 245326 (2006).
[27] P. Mehta and N. Andrei, Phys. Rev. Lett. **96**, 216802 (2006).
[28] B. Doyon, Phys. Rev. Lett. **99**, 076806 (2007).
[29] T. Fujii and K. Ueda, Phys. Rev. B **68**, 155310 (2003).
[30] S. G. Jakobs, V. Meden, and H. Schoeller, Phys. Rev. Lett. **99**, 150603 (2007).
[31] S. Weiss, J. Eckel, M. Thorwart, and R. Egger, Phys. Rev. B **77**, 195316 (2008).
[32] M. Grobis, I. G. Rau, R. M. Potok, H. Shtrikman, and D. Goldhaber-Gordon, arXiv:0710.3211 (unpublished).
[33] S. R. White, Phys. Rev. Lett. **69**, 2863 (1992).
[34] S. R. White, Phys. Rev. B **48**, 10345 (1993).
[35] U. Schollwöck, Rev. Mod. Phys. **77**, 259 (2005).
[36] K. Hallberg, Advances in Physics **55**, 477 (2006).
[37] A. Daley, C. Kollath, U. Schollwöck, and G. Vidal, J. Stat. Mech.: Theory Exp. (2004) P04005.
[38] S. R. White and A. E. Feiguin, Phys. Rev. Lett. **93**, 076401 (2004).
[39] W. Hofstetter, Phys. Rev. Lett. **85**, 1508 (2000).
[40] S. Nishimoto and E. Jeckelmann, J. Phys.: Condens. Matter **16**, 613 (2004).
[41] A. Weichselbaum, F. Verstraete, U. Schollwöck, J. I. Cirac, and J. von Delft, arXiv:cond-mat/0504305 (unpublished).
[42] H. Saberi, A. Weichselbaum, and J. von Delft, Phys. Rev. B **78**, 035124 (2008).
[43] A. Holzner, A. Weichselbaum, and J. von Delft, arXiv:0804.0550 (unpublished).
[44] E. V. Anda, G. Chiappe, C. A. Büsser, M. A. Davidovich, G. Martins, F. Heidrich-Meisner, and E. Dagotto, Phys. Rev. B **78**, 085308 (2008).
[45] S. Costamagna, C. J. Gazza, M. E. Torio, and J. A. Riera, Phys. Rev. B **74**, 195103 (2006).
[46] D. Bohr, P. Schmitteckert, and P. Wölfle, Europhys. Lett. **73**, 246 (2006).
[47] D. Bohr and P. Schmitteckert, Phys. Rev. B **75**, 241103(R) (2007).
[48] P. Nordlander, M. Pustilnik, Y. Meir, N. S. Wingreen, and D. C. Langreth, Phys. Rev. Lett. **83**, 808 (1999).
[49] F. Heidrich-Meisner, G. B. Martins, C. A. Büsser, K. A. Al-Hassanieh, A. E. Feiguin, G. Chiappe, E. V. Anda, and E. Dagotto, arXiv:0705.1801 (unpublished).
[50] M. A. Cazalilla and J. B. Marston, Phys. Rev. Lett. **88**, 256403 (2002).
[51] F. B. Anders and A. Schiller, Phys. Rev. B **74**, 245113 (2006).
[52] W. C. Oliveira and L. N. Oliveira, Phys. Rev. B **49**, 11986 (1994).
[53] G. De Chiara, S. Montangero, P. Calabrese, and R. Fazio, J. Stat. Mech.: Theory Exp. (2006) P03001.
[54] P. Calabrese and J. Cardy, J. Stat. Mech.: Theory Exp. (2007) P06008.
[55] H. R. Krishna-murthy, J. W. Wilkins, and K. G. Wilson, Phys. Rev. B **21**, 1003 (1980).
[56] T_K is calculated within NRG in units of the half-bandwidth D of the leads. A comparison of the parameters entering NRG and DMRG calculations can be made by identifying $D = 2t_0$ where t_0 is the tight-binding hopping in the DMRG chain in the continuum limit and $\Lambda = 1$.
[57] K. Schönhammer, Phys. Rev. B **75**, 205329 (2007) and private communication.
[58] D. Gobert, C. Kollath, U. Schollwöck, and G. Schütz, Phys. Rev. E **71**, 036102 (2005).